

1 **Comparison of Water Vapor Measurements by Airborne Sun Photometer and**  
2 **Diode Laser Hygrometer on the NASA DC-8**  
3  
4

5 J. M. LIVINGSTON<sup>a</sup>, B. SCHMID<sup>b</sup>, P. B. RUSSELL<sup>c</sup>, J. REDEMANN<sup>d</sup>, J. R. PODOLSKÉ<sup>c</sup>, G. S. DISKIN<sup>e</sup>  
6  
7

8 For submittal to *J. Atmos. Oceanic Technol.*

9 13 July 2007  
10

11 Corresponding author:  
12 John M. Livingston  
13 SRI International  
14 333 Ravenswood Avenue  
15 Menlo Park, CA 94025 U.S.A.  
16 Phone: +1 650 859 4174  
17 Fax: +1 650 322 3218  
18 e-mail: john.livingston@sri.com  
19

20  
21 <sup>a</sup>*SRI International, 333 Ravenswood Ave., Menlo Park, CA 94025 USA*

22 <sup>b</sup>*Pacific Northwest National Laboratory, 902 Battelle Boulevard, Richland WA 99352 USA*

23 <sup>c</sup>*NASA Ames Research Center, MS 245-5, Moffett Field, CA 94035-1000 USA*

24 <sup>d</sup>*Bay Area Environmental Research Institute, 560 Third St. West, Sonoma, CA 95476 USA*

25 <sup>e</sup>*NASA Langley Research Center, Hampton, VA 23681-2199 USA*  
26  
27

27

## ABSTRACT

28 In January-February 2003 the 14-channel NASA Ames Airborne Tracking Sunphotometer  
29 (AATS) and the NASA Langley/Ames Diode Laser Hygrometer (DLH) were flown on the  
30 NASA DC-8 aircraft. AATS measured column water vapor on the aircraft-to-sun path, while  
31 DLH measured local water vapor in the free stream between the aircraft fuselage and an  
32 outboard engine cowling. The AATS and DLH measurements were compared for two DC-8  
33 vertical profiles by differentiating the AATS column measurement and/or integrating the DLH  
34 local measurement over the altitude range of each profile (7.7-10 km and 1.2-12.5 km). These  
35 comparisons extend, for the first time, tests of AATS water vapor retrievals to altitudes  $>\sim 6$  km  
36 and column contents  $<0.1 \text{ g cm}^{-2}$ . To our knowledge this is the first time suborbital spectroscopic  
37 water vapor measurements using the 940-nm band have been tested in conditions so high and  
38 dry. For both profiles layer water vapor (LWV) from AATS and DLH were highly correlated,  
39 with  $r^2$  0.998, rms difference 7.2% and bias (AATS minus DLH) 0.9%. For water vapor densities  
40 AATS and DLH had  $r^2$  0.968, rms difference 27.6%, and bias (AATS minus DLH) -4.2%. These  
41 results compare favorably with previous comparisons of AATS water vapor to in situ results for  
42 altitudes  $<\sim 6$  km, columns  $\sim 0.1$  to  $5 \text{ g cm}^{-2}$  and densities  $\sim 0.1$  to  $17 \text{ g m}^{-3}$ .

43 **1. Introduction**

44 Water vapor measurements by sunphotometry using the 940-nm water vapor absorption  
45 band have been compared to in situ and other remote (e.g., microwave) measurements in several  
46 previous publications (e.g., Schmid et al. 2000, 2001, 2003a,b, 2006; Redemann et al. 2003;  
47 Livingston et al. 2000, 2003, 2007). Those comparisons were all restricted to sunphotometer

48 altitudes  $< \sim 6$  km, with water vapor columns  $\sim 0.1$  to  $5 \text{ g cm}^{-2}$  and water vapor densities  $\sim 0.1$  to  
49  $17 \text{ g m}^{-3}$ .

50 In January-February 2003, the 14-channel NASA Ames Airborne Tracking Sunphotometer  
51 (AATS) flew on the DC-8 along with the NASA Langley/Ames Diode Laser Hygrometer  
52 (DLH). The flights were part of the second SAGE (Stratospheric Aerosol and Gas Experiment)  
53 III Ozone Loss and Validation Experiment (SOLVE II). They provided an opportunity to test  
54 AATS water vapor measurements in higher, drier environments, including altitudes up to 12 km  
55 and water vapor columns  $\sim 0.002$  to  $0.1 \text{ g cm}^{-2}$  above 4 km. The availability of DLH  
56 measurements on the same aircraft as AATS provided an especially good comparison  
57 opportunity, since the DLH was designed and built to perform well in environments this high and  
58 dry, and previous DLH measurements had been compared to other state-of-the-art water vapor  
59 measurements in such regions (e.g., Podolske et al. 2003). To our knowledge there had not been  
60 any previous tests of suborbital spectroscopic water vapor measurements using the 940-nm band  
61 in conditions so high and dry.

62 It should be noted, however, that several satellite instruments that view the sun through the  
63 Earth's atmospheric limb do use the 940-nm band for water vapor measurements, and they have  
64 been validated. These instruments include the Stratospheric Aerosol and Gas Experiment  
65 (SAGE) and Polar Ozone and Aerosol Measurement (POAM) families of sensors, validations of  
66 which have been published by, e.g., Nedoluha et al. (2002), Taha et al. (2004), Thomason et al.  
67 (2004), and Lumpe et al. (2006). The SAGE and POAM measurements benefit from the long  
68 viewing path of their limb-viewing geometry (e.g.,  $\sim 200$  km in a 1-km thick atmospheric shell,  
69 resulting from local solar zenith angle  $\sim 90^\circ$ ), which produces measurable absorption in the 940-

70 nm band even for stratospheric concentrations of water vapor (typically 3-8 ppmv). The AATS  
71 DC-8 measurements reported in this paper had true solar zenith angle ranging from 68.6° to  
72 89.1°, which includes viewing paths (hence airmass factors) considerably less than those for the  
73 SAGE and POAM viewing geometries.

## 74 **2. Instruments and Data Analysis Techniques**

### 75 *a. 14-channel Ames Airborne Tracking Sunphotometer (AATS)*

76 The 14-channel NASA Ames Airborne Tracking Sunphotometer (AATS-14 or simply  
77 AATS in this paper) has been described previously in the literature (e.g., Russell et al. 2005,  
78 2007), so we give only a brief synopsis here. AATS measures the direct beam solar transmission  
79 in 14 channels with center wavelengths from 354 to 2138 nm, including a channel centered at  
80 941 nm. Azimuth and elevation motors rotate a tracking head to lock on to the solar beam and  
81 maintain detectors normal to it.

82 The AATS channel wavelengths are chosen to permit separation of aerosol, water vapor,  
83 and ozone transmission along the measured slant path. Our methods for data reduction,  
84 calibration, and error analysis have been described in detail previously (Russell et al. 1993a,  
85 1993b; Schmid and Wehrli 1995; Schmid et al. 1996, 2001, 2003). Water vapor analysis  
86 methods are briefly reviewed below. Results for AATS aerosol optical depth and ozone  
87 measurements from the DC-8 in SOLVE II are described by Russell et al. (2005) and Livingston  
88 et al. (2005).

89 AATS was calibrated by analysis of sunrise measurements acquired at Mauna Loa  
90 Observatory (MLO), Hawaii, for six sunrises in November 2002 prior to SOLVE II and for

91 seven sunrises in March 2003 after SOLVE II. Exoatmospheric detector voltages,  $V_0$ , were  
 92 derived using the Langley plot technique (e.g., Russell et al. 1993a, 1993b; Schmid and Wehrli  
 93 1995) for all channels except 941 nm, for which a modified Langley technique (Reagan et al.  
 94 1995; Michalsky et al. 1995; Schmid et al. 1996, 2001) was employed to account for water vapor  
 95 absorption.

96 Because absorption by water vapor varies strongly within the 5-nm FWHM bandpass of the  
 97 AATS-14 channel centered at 941 nm, the usual Beer-Lambert-Bouguer expression must be  
 98 modified to describe correctly the relationship between the output detector voltage,  $V(941)$ , and  
 99 the atmospheric attenuators on the sun-to-instrument path. In particular,

$$100 \quad V(941 \text{ nm}) = V_0(941 \text{ nm}) d^{-2} \exp\left[-\sum_i m_i \tau_i(941 \text{ nm})\right] T_w, \quad (1)$$

101 where  $V_0(941 \text{ nm})$  is the exoatmospheric calibration voltage,  $d$  is the Earth-Sun distance in  
 102 astronomical units at the time of observation,  $m_i$  is the airmass factor (ratio of slant path optical  
 103 depth to vertical optical depth) for attenuating species  $i$  (where  $i$  represents gas scattering, non-  
 104 water vapor gas absorption, or aerosol extinction),  $\tau_i$  is the optical depth for the  $i$ th attenuating  
 105 species other than water vapor, and  $T_w$  is the water vapor transmittance (weighted by absorption  
 106 strength, source intensity and filter function). Consistent with the approach followed by  
 107 Livingston et al. (2007), we used the three-parameter expression of Ingold et al. (2000) to  
 108 parameterize  $T_w$  as a function of the amount of water vapor,  $w_s$ , along the slant path:

$$109 \quad T_w = c \exp(-aw_s^b). \quad (2)$$

110 In this expression, the coefficients a, b, and c are least squares fitting parameters. In particular,  
111 calculations were performed using the radiative transfer code LBLRTM V9.2 (Clough et al.  
112 2005) for a variety of model atmospheres and a range of solar zenith angles to extend the  
113 Livingston et al. (2007) Table 2 results to include all altitudes (maximum of ~12.5 km) flown by  
114 the DC-8 during SOLVE II. These results are shown in Fig. 1 and the complete set of fitting  
115 coefficients is given in Table 1.

116 As noted by Livingston et al. (2007) and illustrated here in Fig. 1, a retrieval that ignores  
117 the instrument altitude can result in an incorrect determination of slant path (hence, column)  
118 water vapor. In particular, if it is assumed that the instrument is located at sea level, then column  
119 water vapor (CWV) would be underestimated for instrument altitudes above sea level, and the  
120 errors would be greatest for large solar zenith angles, SZA (high airmass values), and high CWV  
121 (hence, high slant water vapor) amounts.

122 Column water vapor is calculated from the slant amount by dividing by an appropriate  
123 water vapor airmass factor. These airmass factors were calculated using the methodology  
124 reported in Russell et al. (2005) and Livingston et al. (2005) by assuming a vertical water vapor  
125 distribution corresponding to the subarctic winter atmospheric model for the 21 January 2003  
126 measurements and the midlatitude winter atmospheric model for the 6 February 2003 data. The  
127 uncertainty in CWV is computed following Schmid et al. (1996). The calculated CWV values are  
128 averaged within 50-m vertical bins, and a smoothing spline is then fit to the resultant CWV  
129 profile. Water vapor density ( $\rho_w$ ) is obtained as the derivative of the spline fit.

130  
131 *b. Diode Laser Hygrometer*

132 The NASA Langley/Ames Diode Laser Hygrometer (DLH) was designed and built to  
133 measure gas-phase water in the free-stream region of the NASA DC-8 aircraft, between the  
134 fuselage and the cowling of an outboard engine. The instrument is described in detail elsewhere  
135 (Vay et al. 1998; Diskin et al. 2002; Podolske et al. 2003), so only a brief description is given  
136 here.

137 The DLH instrument is a near-infrared (NIR) spectrometer operating at wavelengths near  
138 1.4  $\mu\text{m}$  to detect individual rotation-vibration lines of  $\text{H}_2\text{O}$  in either the (101) combination band  
139 or the (200) overtone band. Second harmonic detection (Sachse et al. 1977, 1987; Reid and  
140 Labrie 1981; Podolske and Loewenstein 1993, and references therein) and long path length are  
141 utilized to achieve high sensitivity, and two or more lines of different strengths are used to meet  
142 the dynamic range requirements for atmospheric water. The beam of a NIR diode laser is  
143 quasicollimated and transmitted through a quartz window secured in a DC-8 window plate,  
144 toward the cowling of the right (starboard) side outboard engine. There it strikes a sheet of  
145 retroreflector material and returns to the fuselage window from which it originally emerged.  
146 Inside the window a portion of the return beam is passed through a narrowband interference  
147 filter, collected by a Fresnel lens, and focused onto a detector. The sample volume of the external  
148 path is completely exchanged every 40–70 ms, depending on aircraft velocity. The laser  
149 wavelength is modulated, and the signal detector output is synchronously demodulated to  
150 produce the second harmonic signal. The second harmonic (2F) and DC components from the  
151 signal detector are recorded to allow power normalizing of the (2F) signal.

152 The laser radiation emitted from the rear facet of the diode laser is sent through a short (50  
153 mm) reference cell containing pure water vapor and onto a second detector. The reference

154 detector output is synchronously demodulated at the third harmonic (3F), the central zero  
155 crossing of which is subsequently used to lock the laser wavelength to the center of the chosen  
156 absorption line.

157 DLH calibration and data retrieval algorithms are described by Podolske et al. (2003).  
158 During SOLVE-II and subsequently, efforts to quantify DLH accuracy have yielded a typical  
159 uncertainty of  $\pm 5\%$ , with a precision at 5 ppmv water vapor of approximately 1%.

160

### 161 **3. Results**

162 Results from the first comparison profile, which was flown 21 January 2003 on a DC-8  
163 ascent out of Kiruna, Sweden, are presented in Fig. 2. AATS was able to view the sun at DC-8  
164 altitudes between  $\sim 7.7$  and 10 km, thus allowing calculation of CWV at each altitude in that  
165 range. The AATS and DLH CWV profiles are overplotted in Fig. 2a, in addition to the ambient  
166 atmospheric temperature profile. Because DLH measures local (not column) water vapor, the  
167 DLH CWV value at profile top is set equal to the AATS value there, and DLH CWV values  
168 below that altitude are obtained by integrating DLH local values downward. Corresponding  
169 AATS and DLH water vapor densities are overplotted in Fig. 2b. As noted in Section 2a, AATS  
170  $\rho_w$  is obtained as the vertical derivative of a spline fit to the AATS CWV profile that results after  
171 averaging the CWV values within 50-m vertical bins.

172 Scatter plot comparisons of AATS and DLH CWV and  $\rho_w$  for the 21 January profile are  
173 shown in Fig. 2c and 2d. The statistics shown on each scatter plot quantify the correlation and  
174 agreement between the AATS and DLH results. For CWV, AATS and DLH have  $r^2$  0.977, rms  
175 difference 13.0% and bias (AATS minus DLH) 8.1%. Corresponding values for  $\rho_w$  are  $r^2$  0.887,

176 rms difference 92.1% and bias (AATS minus DLH) 37.3%. This agreement is noteworthy in  
 177 light of the very dry conditions: maximum AATS CWV of  $0.007 \text{ g cm}^{-2}$  and maximum  $\rho_w$  of  $0.1$   
 178  $\text{g m}^{-3}$ .

179 Fig. 3 shows results from the second comparison profile, which was flown 6 February 2003  
 180 as the DC-8 descended into Edwards Air Force Base, California, on its return from Sweden. In  
 181 this case, AATS was able to view the sun at DC-8 altitudes from  $\sim 12.5$  km to the surface. This  
 182 profile is noteworthy for combining very dry conditions above  $\sim 6$  km (similar to those in the 21  
 183 January case, cf. Fig. 2) with significantly increased CWV and  $\rho_w$ , and strong vertical structure,  
 184 below  $\sim 6$  km (though values are still small compared to the previous AATS comparisons cited in  
 185 Section 1). Another significant feature of this profile is the availability of water vapor data from  
 186 the radiosonde released from Edwards at 1500 UT (1.5 to 1.9 h before the DC-8 descent profile).  
 187 Frames 3a and 3b overplot the results for the entire range of measurement altitudes; frames 3c  
 188 and 3d expand the results between 7.5 and 12.5 km. For this case, in order to minimize the effect  
 189 of horizontal inhomogeneities on the calculated AATS CWV profile, the AATS CWV values  
 190 above 4.5 km were smoothed more than the values below 4.5 km in applying the spline fit.

191 Corresponding values of AATS and DLH CWV and  $\rho_w$  for the 6 February profile are  
 192 compared in scatter plots in Fig. 4. For CWV calculated from the measurements obtained during  
 193 this profile, AATS and DLH have  $r^2$  0.998, rms difference 6.6% and bias (AATS minus DLH)  
 194 0.8%. Corresponding values for  $\rho_w$  are  $r^2$  0.965, rms difference 25.2% and bias (AATS minus  
 195 DLH) -4.8%. Even for comparisons between AATS and the sonde, which was flown 1.5-1.9 h  
 196 earlier, the overall agreement is striking: for AATS values interpolated to sonde-reported  
 197 altitudes, AATS and sonde CWV have  $r^2$  0.997, rms difference 15.1% and bias (AATS minus

198 sonde) 6.3%. Corresponding values for  $\rho_w$  are  $r^2$  0.897, rms difference 42.7% and bias (AATS  
 199 minus sonde) 10.4%. The maxima of the scatter plots ( $CWV < 0.3 \text{ g cm}^{-2}$ ,  $\rho_w < 1.1 \text{ g m}^{-3}$ ), though  
 200 larger than those shown in Fig. 2, are still noteworthy for their small values. For example, in  
 201 previous AATS comparisons to in situ and other remote water vapor measurements, CWV has  
 202 ranged up to  $\sim 5 \text{ g cm}^{-2}$  and  $\rho_w$  up to  $\sim 17 \text{ g m}^{-3}$ .

203 Fig. 5 shows scatter plots that combine AATS and DLH results for the profiles on 21  
 204 January and 6 February. AATS and DLH CWV (5a) have  $r^2$  0.998, rms difference 7.2% and bias  
 205 (AATS minus DLH) 0.9%. Corresponding values for  $\rho_w$  (5b) are  $r^2$  0.968, rms difference 27.6%  
 206 and bias (AATS minus DLH) -4.2%. Results for altitudes  $> 7.5 \text{ km}$  only are shown for CWV and  
 207  $\rho_w$  in 5c and 5d, respectively. For CWV, values are  $r^2$  0.971, rms difference 9.4% and bias  
 208 (AATS minus DLH) -4.2%. For  $\rho_w$ , values are  $r^2$  0.910, rms difference 73.6% and bias (AATS  
 209 minus DLH) 26.5%.

210 These values are similar to those found in previous AATS-14 water vapor comparisons (as  
 211 cited in the introduction) with much larger CWV and  $\rho_w$ . Most recently, Livingston et al. (2007)  
 212 compared layer water vapor (LWV) between profile top and bottom as measured by AATS and  
 213 an in situ sensor on the same aircraft during 35 vertical profiles acquired over the Gulf of Maine,  
 214 with maximum LWV  $\sim 3.7 \text{ g cm}^{-2}$  and maximum  $\rho_w \sim 16 \text{ g m}^{-3}$ . They found  $r^2$  0.97, rms  
 215 difference 8.8% and bias (AATS minus in situ) -7.1%. For 22 profiles within 1 h and 130 km of  
 216 sonde ascents, they found AATS and sonde LWV had  $r^2$  0.90, rms difference 10.7%, and bias  
 217 (AATS minus sonde) -5.4%. Previously, Schmid et al. (2006) reported an AATS dry bias of 5%  
 218 relative to coincident  $\rho_w$  measurements acquired with an Edgetech 137-C3 chilled mirror for 35  
 219 vertical profiles over the Atmospheric Radiation Measurement (ARM) Southern Great Plains

220 (SGP) site. In each of these studies, AATS was equipped with the same 941-nm interference  
221 filter used during SOLVE II.

#### 222 **4. Summary and Conclusions**

223 This paper has compared values of CWV and  $\rho_w$  calculated from simultaneous  
224 measurements acquired by the AATS and DLH sensors on the DC-8 for two vertical profiles  
225 flown during SOLVE II. This study is unique because it includes data acquired at altitudes  
226 (above 6 km) where we had previously never taken measurements and where the amount of  
227 water vapor in the atmosphere was the lowest we have ever measured. To our knowledge this is  
228 the first time suborbital spectroscopic water vapor measurements using the 940-nm water vapor  
229 absorption band have been tested in conditions so high and dry.

230 Measurements were acquired at altitudes between 7.7 km and 10 km during the 21 January  
231 aircraft ascent, and between 1.1 km and 12.5 km during the 6 February descent. AATS and DLH  
232 CWV values (where the DLH value was set equal to the AATS CWV value at the top of the  
233 profile) yielded  $r^2$  of 0.997 for 21 January and 0.998 for 6 February. Comparison of AATS and  
234 radiosonde CWV values for sonde measurements (normalized to AATS CWV at the top of the  
235 profile) acquired 1.5-1.9 h before the AATS profile on 6 February yielded an  $r^2$  of 0.997. For  
236 measurements taken at altitudes  $>7.5$  km, the composite AATS and DLH data set gave an  $r^2$  of  
237 0.97, an rms difference of 9.4% ( $0.0004 \text{ g cm}^{-2}$ ), and a bias (AATS minus DLH) of 4.2% ( $0.0002$   
238  $\text{g cm}^{-2}$ ). Corresponding values for  $\rho_w$  were  $r^2$  of 0.91, an rms difference of 73.6% ( $0.01 \text{ g m}^{-3}$ ),  
239 and a bias (AATS minus DLH) of 26.5% ( $0.004 \text{ g m}^{-3}$ ). The large relative rms and bias  
240 differences reflect the dry atmosphere with  $\rho_w < 0.1 \text{ g m}^{-3}$  at those altitudes.

241           The comparisons presented here included a very limited set of measurements at altitudes in  
242 the 7-12 km range, and additional comparisons between sunphotometer and in situ sensors are  
243 needed at these altitudes where the amount of water vapor in the atmosphere is so low to permit  
244 quantification of the uncertainty in the sunphotometer-calculated  $\rho_w$  values. Nevertheless, the  
245 agreement we have found between the AATS and DLH retrievals of CWV (essentially, LWV)  
246 gives us hope that airborne sunphotometer measurements can provide useful data for validation  
247 of satellite water vapor retrievals not only for the full atmospheric column and for  $\rho_w$  in the  
248 lowest few km of the troposphere, as has been shown in previous studies, but also at altitudes in  
249 the upper troposphere where water vapor is limited.

250  
251  
252  
253  
254  
255  
256

*Acknowledgments.* We thank James Eilers and Richard Kolyer for supporting AATS measurements, and Stephanie Ramirez for help with illustrations and formatting. The SOLVE II measurements were supported by NASA's Upper Atmosphere Research Program. AATS analyses were supported by NASA's Solar Occultation Satellite Science Team.

## REFERENCES

- 256  
257  
258 Clough, S.A., M.W. Shephard, E.J. Mlawer, J.S. Delamere, M.J. Iacono, K. Cady-Pereira, S.  
259 Boukabara, and P.D. Brown, 2005: Atmospheric radiative transfer modeling: a summary of  
260 the AER codes. *Journal of Quantitative Spectroscopy and Radiative Transfer*, **91**, 233-244.
- 261 Diskin, G. S., J. R. Podolske, G. W. Sachse, and T. A. Slate, 2002: Open-path airborne tunable  
262 diode laser hygrometer. *Proc. of Soc. of Photoopt. Instrum. Eng.*, **4817**, 196-204,  
263 doi:10.1117/12.453736.
- 264 Ingold, T., B. Schmid, C. Matzler, P. Demoulin, and N. Kampfer, 2000: Modeled and empirical  
265 approaches for retrieving columnar water vapor from solar transmittance measurements in  
266 the 0.72, 0.82, and 0.94 mm absorption bands. *J. Geophys. Res.*, **105**, D19, 24,327,  
267 2000JD900392.
- 268 Livingston, J. M., V. Kapustin, B. Schmid, P. B. Russell, P. A. Durkee, T. Bates, and P. K.  
269 Quinn, 2000: Shipboard sunphotometer measurements of aerosol optical depth spectra and  
270 columnar water vapor during ACE-2, and comparison with selected land, ship, aircraft, and  
271 satellite measurements, *Tellus B*, **52**, 594-619.
- 272 Livingston, J. M., P. B. Russell, J. S. Reid, J. Redemann, B. Schmid, D. A. Allen, O. Torres, R.  
273 C. Levy, L. A. Remer, B. N. Holben, A. Smirnov, O. Dubovik, E. J. Welton, J. R. Campbell,  
274 J. Wang, and S. A. Christopher, 2003: Airborne Sun photometer measurements of aerosol  
275 optical depth and columnar water vapor during the Puerto Rico Dust Experiment and  
276 comparison with land, aircraft, and satellite measurements. *J. Geophys. Res.*, **108**, D19,  
277 doi:10.1029/2002JD002520.
- 278 Livingston, J. M., B. Schmid, P. B. Russell, J. A. Eilers, R. W. Kolyer, J. Redemann, S. A.  
279 Ramirez, J.-H. Yee, W. H. Swartz, C. R. Trepte, L. W. Thomason, M. C. Pitts, M. A. Avery,

- 280 C. E. Randall, J. D. Lumpe, R. M. Bevilacqua, M. Bittner, T. Erbertseder, R. D. McPeters, R.  
281 E. Shetter, E. V. Browell, J. B. Kerr, and K. Lamb, 2005: Retrieval of ozone column content  
282 from airborne Sun photometer measurements during SOLVE II: comparison with coincident  
283 satellite and aircraft measurements. *Atmos. Chem. Phys.*, **5**, 1-20.
- 284 Livingston, J., B. Schmid, J. Redemann, P. Russell, S. Ramirez, J. Eilers, W. Gore, S. Howard, J.  
285 Pommier, E. Fetzer, S. Seeman, E. Borbas, D. Wolfe, and A. M. Thompson, 2007:  
286 Comparison of water vapor measurements by airborne Sun photometer and near-coincident  
287 in situ and satellite sensors during INTEX/ITCT 2004. *J. Geophys. Res.*, **112**, D12S16,  
288 doi:10.1029/2006JD007733.
- 289 Lumpe, J., R. Bevilacqua, C. Randall, G. Nedoluha, K. Hoppel, J. Russell, V. L. Harvey, C.  
290 Schiller, B. Sen, G. Taha, G. Toon, and H. Vömel, 2006: Validation of Polar Ozone and  
291 Aerosol Measurement (POAM) III version 4 stratospheric water vapor. *J. Geophys. Res.*,  
292 **111**, D11301, doi:10.1029/2005JD006763.
- 293 Michalsky, J. J., J. C. Liljegren, and L. C. Harrison, 1995: A comparison of sun photometer  
294 derivations of total column water vapor and ozone to standard measures of same at the  
295 Southern Great Plains Atmospheric Radiation Measurement site. *J. Geophys. Res.*, **100**,  
296 25,995-26,003.
- 297 Nedoluha, G. E., R. M. Bevilacqua, K. W. Hoppel, J. D. Lumpe, and H. Smit, 2002: Polar Ozone  
298 and Aerosol Measurement III measurements of water vapor in the upper troposphere and  
299 lowermost stratosphere. *J. Geophys. Res.*, **107**(D10), 4103, doi:10.1029/2001JD000793.
- 300 Podolske, J., and M. Loewenstein, 1993: Airborne tunable diode laser spectro-meter for trace-gas  
301 measurement in the lower stratosphere. *Appl. Opt.*, **32**, 5324-5333.

- 302 Podolske, J. R., G. W. Sachse, and G. S. Diskin, 2003: Calibration and data retrieval algorithms  
 303 for the NASA Langley/Ames Diode Laser Hygrometer for the NASA Transport and  
 304 Chemical Evolution Over the Pacific (TRACE-P) mission. *J. Geophys. Res.*, **108**(D20),  
 305 8792, doi:10.1029/2002JD003156.
- 306 Reagan, J., K. Thome, B. Herman, R. Stone, J. Deluisi, and J. Snider, 1995: A comparison of  
 307 columnar water-vapor retrievals obtained with near-IR solar radiometer and microwave  
 308 radiometer measurements. *J. Appl. Meteorol.*, **34**, 1384-1391.
- 309 Reid, J., and D. Labrie, 1981: Second-harmonic detection with tunable diode lasers—Comparison  
 310 of experiment and theory. *Appl. Phys.*, **B26**, 203 –210.
- 311 Redemann, J., S. Masonis, B. Schmid, T. Anderson, P. Russell, J. Livingston, O. Dubovik, A.  
 312 Clarke, 2003: Clear-column closure studies of aerosols and water vapor aboard the NCAR C-  
 313 130 in ACE-Asia, 2001. *J. Geophys. Res.*, **108**(D23), 8655, doi:10.1029/2003JD003442.
- 314 Russell, P. B., J. M. Livingston, E. G. Dutton, R. F. Pueschel, J. A. Reagan, T. E. DeFoor, M. A.  
 315 Box, D. Allen, P. Pilewskie, B. M. Herman, S. A. Kinne, and D. J. Hofmann, 1993a:  
 316 Pinatubo and pre-Pinatubo optical-depth spectra: Mauna Loa measurements, comparisons,  
 317 inferred particle size distributions, radiative effects, and relationship to lidar data. *J.*  
 318 *Geophys. Res.*, **98**, 22,969-22,985.
- 319 Russell, P. B., J. M. Livingston, R. F. Pueschel, J. A. Reagan, E. V. Browell, G. C. Toon, P. A.  
 320 Newman, M. R. Schoeberl, L. R. Lait, L. Pfister, Q. Gao, and B. M. Herman, 1993b: Post-  
 321 Pinatubo optical depth spectra vs. latitude and vortex structure: Airborne tracking  
 322 sunphotometer measurements in AASE II. *Geophys. Res. Lett.*, **20**, 2571-2574.
- 323 Russell, P., J. Livingston, B. Schmid, J. Eilers, R. Kolyer, J. Redemann, S. Ramirez, J-H. Yee,  
 324 W. Swartz, R. Shetter, C. Trepte, L. Thomason, A. Risley, Jr., B. Wenny, J. Zawodny, W.

- 325 Chu, M. Pitts, J. Lumpe, C. Randall, and R. Bevilacqua, 2005: Aerosol optical depth  
326 measurements by airborne sun photometer in SOLVE II: Comparison to SAGE III, POAM  
327 III and airborne spectrometer measurements. *Atmos. Chem. Phys.*, **5**, 1-29.
- 328 Russell, P. B., J. M. Livingston, J. Redemann, B. Schmid, S. A. Ramirez, J. Eilers, R. Kahn, A.  
329 Chu, L. Remer, P. K. Quinn, M. J. Rood, and W. Wang, Multi-grid-cell validation of satellite  
330 aerosol property retrievals in INTEX/ITCT/ICARTT 2004, 2007: *J. Geophys. Res.*, **112**,  
331 D12S09, doi:10.1029/2006JD007606.
- 332 Sachse, G. W., G. F. Hill, L. O. Wade, and E. P. Condon, 1977: DACOM-A rapid, high  
333 sensitivity airborne carbon monoxide monitor. Proceedings of the Fourth Joint Conference  
334 on Sensing of Environmental Pollutants, edited by H. G. Stewart, 590 – 593, Am. Chem.  
335 Soc., Washington, DC.
- 336 Sachse, G. W., G. F. Hill, L. O. Wade, and M. G. Perry, 1987: Fast-response, high-precision  
337 carbon monoxide sensor using a tunable diode laser absorption technique, *J. Geophys. Res.*,  
338 **92**, 2071– 2081.
- 339 Schmid, B., and C. Wehrli, 1995: Comparison of sun photometer calibration by Langley  
340 technique and standard lamp. *Appl. Opt.*, **34**, 4500-4512.
- 341 Schmid, B., K. J. Thome, P. Demoulin, R. Peter, C. Mätzler, and J. Sekler, 1996: Comparison of  
342 modeled and empirical approaches for retrieving columnar water vapor from solar  
343 transmittance measurements in the 0.94- $\mu\text{m}$  region. *J. Geophys. Res.*, **101**, 9345-9358.
- 344 Schmid, B., J. M. Livingston, P. B. Russell, et al., 2000: Clear sky closure studies of lower  
345 tropospheric aerosol and water vapor during ACE-2 using airborne sunphotometer, airborne  
346 in-situ, space-borne, and ground-based measurements, *Tellus B*, **52**, 568-593.

- 347 Schmid B., J. J. Michalsky, D. W. Slater, J. C. Barnard, R. N. Halthore, J. C. Liljegren, B. N.  
348 Holben, T. F. Eck, J. M. Livingston, P. B. Russell, T. Ingold, and I. Slutsker, 2001:  
349 Comparison of columnar water-vapor measurements from solar transmittance methods.  
350 *Applied Optics*, **40**, 1886-1896.
- 351 Schmid, B., J. Redemann, P. B. Russell, P. V. Hobbs, D. L. Hlavka, M. J. McGill, B. N. Holben,  
352 E. J. Welton, J. R. Campbell, O. Torres, R. A. Kahn, D. J. Diner, M. C. Helmlinger, D. A.  
353 Chu, C. Robles-Gonzalez, and G. De Leeuw, 2003a: Coordinated airborne, spaceborne, and  
354 ground-based measurements of massive, thick aerosol layers during the dry season in  
355 Southern Africa. *J. Geophys. Res.*, **108** (D13), 8496, doi:10.1029/2002JD002297.
- 356 Schmid, B., D. A. Hegg, J. Wang, D. Bates, J. Redemann, P. B. Russell, J. M. Livingston, H. H.  
357 Jonsson, E. J. Welton, J. H. Seinfeld, R. C. Flagan, D. S. Covert, O. Dubovik, A. Jefferson,  
358 2003b: Column closure studies of lower tropospheric aerosol and water vapor during ACE-  
359 Asia using airborne sunphotometer, airborne in-situ and ship-based lidar measurements. *J.*  
360 *Geophys. Res.*, **108**(D23), 8656, doi:10.10292002JD003361.
- 361 Schmid B., R. Ferrare, C. Flynn, R. Elleman, D. Covert, A. Strawa, E. Welton, D. Turner, H.  
362 Jonsson, J. Redemann, J. Eilers, K. Ricci, A. G. Hallar, M. Clayton, J. Michalsky, A.  
363 Smirnov, B. Holben, J. Barnard, 2006: How well do state-of-the-art techniques measuring the  
364 vertical profile of tropospheric aerosol extinction compare? *J. Geophys. Res.*, **111**, D05S07,  
365 doi:10.1029/2005JD005837.
- 366 Taha, G., L. W. Thomason, and S. P. Burton, 2004: Comparison of Stratospheric Aerosol and  
367 Gas Experiment (SAGE) II version 6.2 water vapor with balloon-borne and space-based  
368 instruments, *J. Geophys. Res.*, **109**, D18313, doi:10.1029/2004JD004859.

369 Thomason, L. W., S. P. Burton, N. Iyer, J. M. Zawodny, and J. Anderson, 2004: A revised water  
370 vapor product for the Stratospheric Aerosol and Gas Experiment (SAGE) II version 6.2 data  
371 set, *J. Geophys. Res.*, **109**, D06312, doi:10.1029/2003JD004465.

372 Vay, S. A., B. E. Anderson, G. W. Sachse, J. E. Collins Jr., J. R. Podolske, C. H. Twohy, B.  
373 Gandrud, K. R. Chan, S. L. Baughcum, and H. A. Wallio, 1998: DC-8-based observations of  
374 aircraft CO, CH<sub>4</sub>, N<sub>2</sub>O, and H<sub>2</sub>O<sub>(g)</sub> emission indices during SUCCESS, *Geophys. Res. Lett.*,  
375 **25**, 1717–1720.

376

376 Table 1. Coefficients of Ingold et al. (2000) 3-parameter functional fit (2-parameter at altitudes  
 377 below 4 km) to LBLRTM\_v9.2 calculations of water vapor transmittance as a function of slant  
 378 path water vapor  $w_s$  (where  $w_s$  is in units of cm or  $g/cm^2$ ) for the AATS-14 channel centered at  
 379 940.6 nm. Values for altitudes 0-8 km are the same as those shown in Table 2 of Livingston et  
 380 al. (2007).

381

<u>Altitude [km]</u>	<u>a</u>	<u>b</u>	<u>c</u>
0	0.51623	0.6439	1.00000
1	0.49669	0.6331	1.00000
2	0.47492	0.6238	1.00000
3	0.45191	0.6186	1.00000
4	0.43700	0.6053	1.00540
5	0.42217	0.5929	1.00924
6	0.40499	0.5859	1.01006
7	0.38888	0.5892	1.00855
8	0.38005	0.6059	1.00614
9	0.38692	0.6354	1.00394
10	0.43234	0.6897	1.00195
11	0.53860	0.7600	1.00077
12	0.60497	0.7952	1.00040
13	0.33551	0.6835	1.00086

382

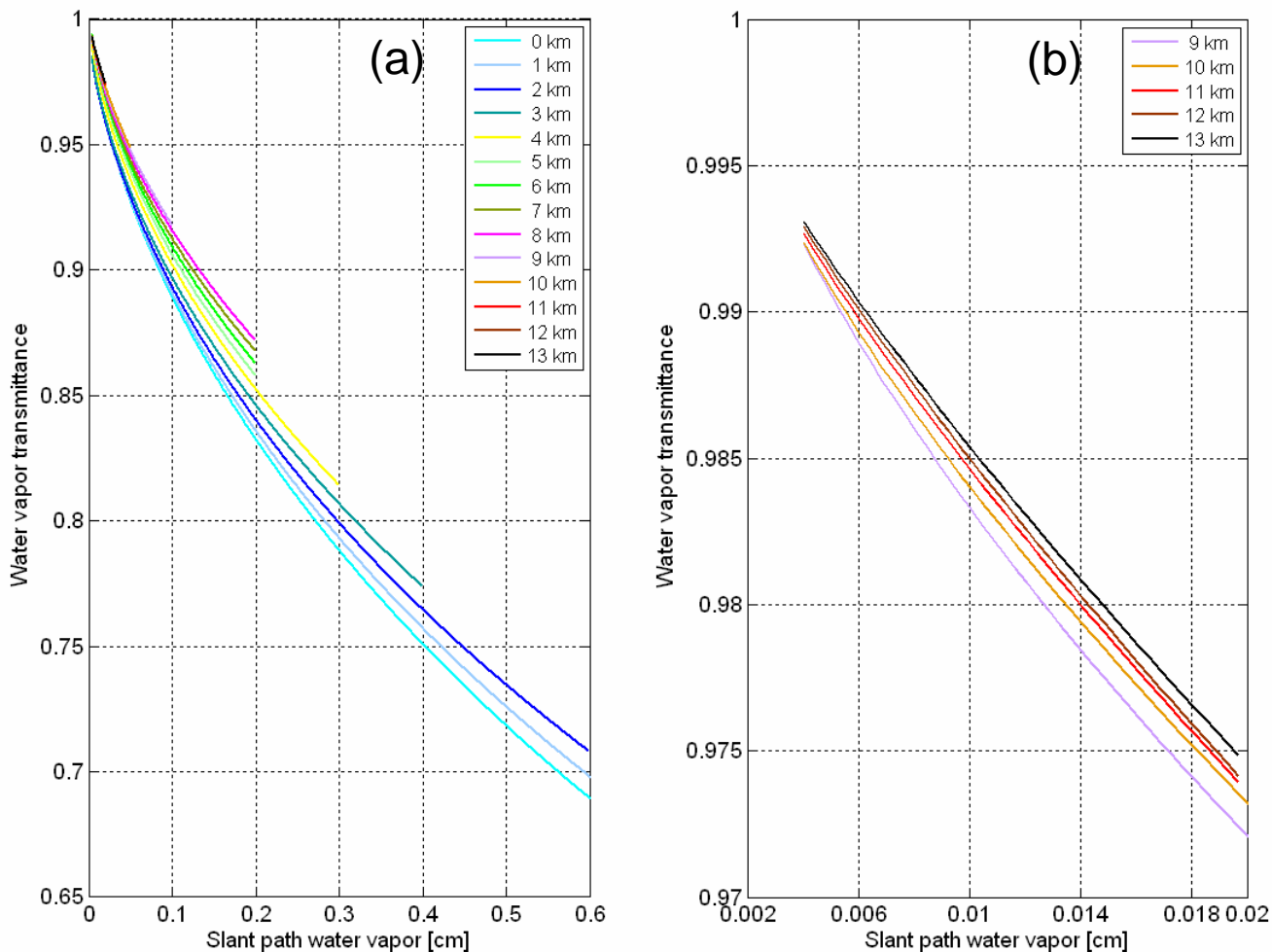


**Fig. 1.** LBLRTM calculations of water vapor transmittance  $T_w$  as a function of slant path water vapor and aircraft (instrument) altitude for the AATS-14 941-nm channel. Results are shown for altitudes from 0 to 13 km in (a) and on expanded axes for altitudes 9 to 13 km only in (b).

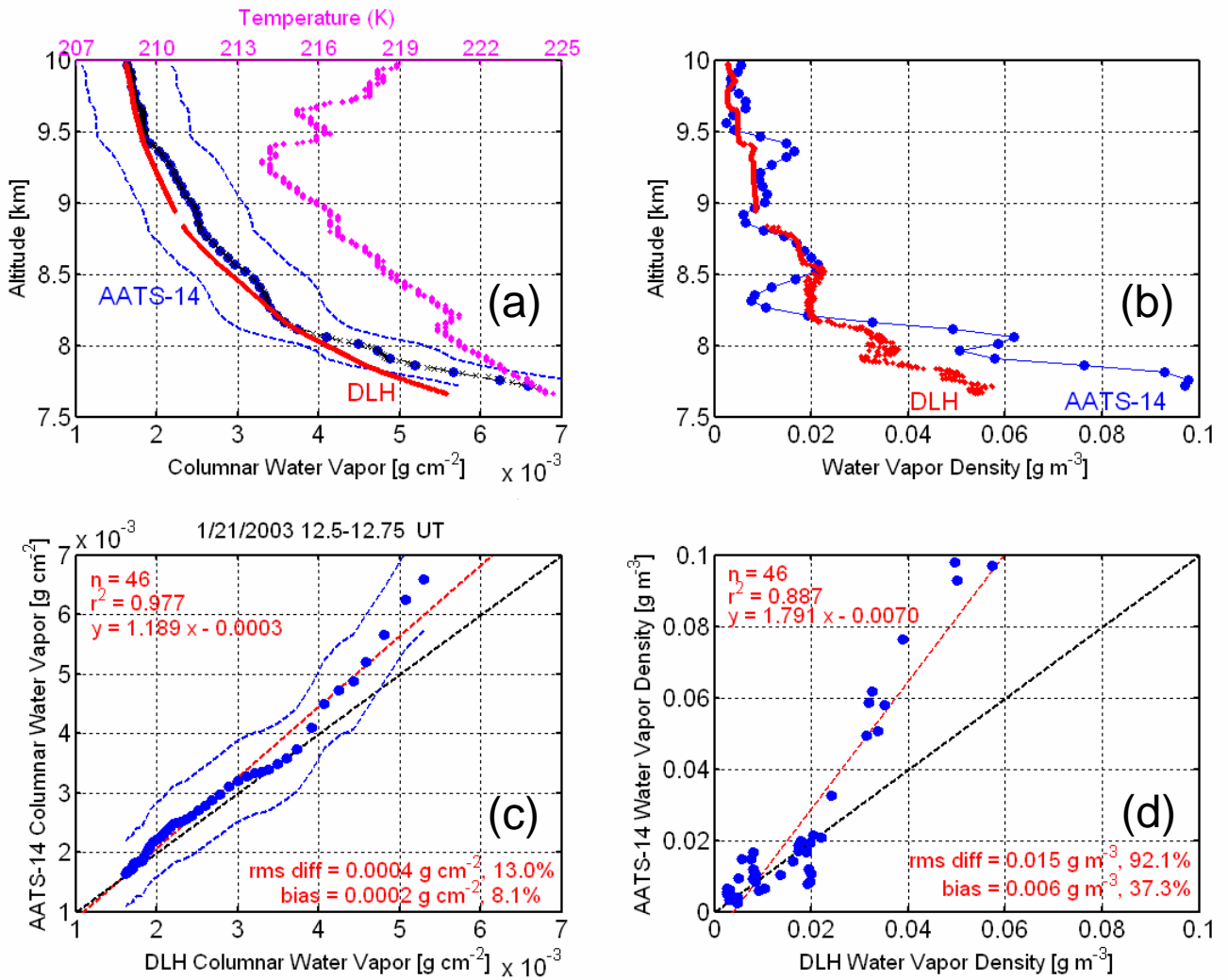


**Fig. 2.** For the 21 January 2003 DC-8 ascent out of Kiruna, Sweden, (a) profiles of AATS-14 unbinned (black xs) and binned (blue dots) CWV, AATS-14 one sigma CWV uncertainties (dashed blue lines), DLH CWV (red dots), and ambient atmospheric temperature (magenta dots); (b) corresponding profiles of AATS-14 and DLH water vapor density; (c) scatterplot of AATS-14 versus DLH CWV (blue dots), AATS-14 CWV uncertainties (dashed blue lines), and linear regression fit (red line); (d) scatterplot of AATS-14 versus DLH water vapor density, and linear regression fit (red line). For CWV, the DLH value at profile top has been set equal to the AATS value there. Black dashed line in (c) and in (d) represents the one-to-one correspondence.

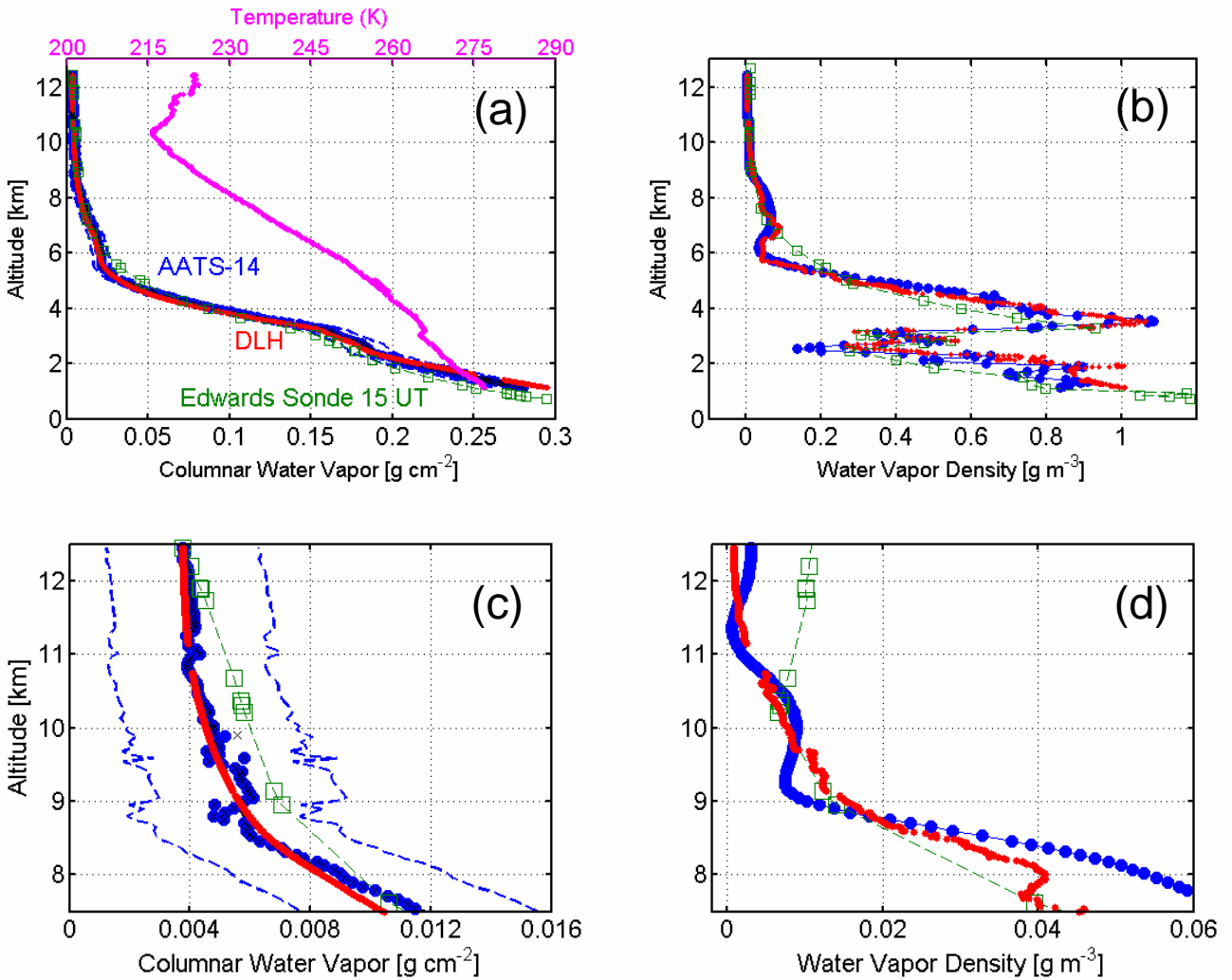


**Fig. 3.** For the 6 February 2003 DC-8 descent into Edwards AFB, (a) profiles of AATS-14 CWV (blue dots), AATS-14 one sigma CWV uncertainties (dashed blue lines), DLH CWV (red dots), CWV (green squares) calculated from Edwards AFB 15 UT radiosonde, and ambient atmospheric temperature (magenta dots); (b) corresponding profiles of water vapor density; (c,d) same profiles shown in (a,b), but for altitudes above 7.5 km only with expanded axes limits. For CWV, the DLH and sonde values at profile top have been set equal to the AATS value there.

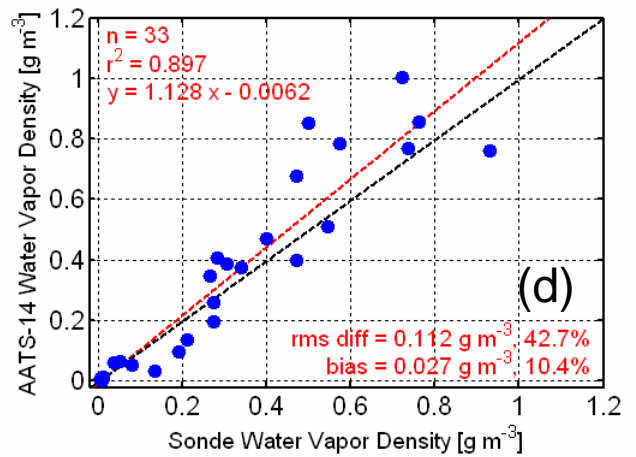
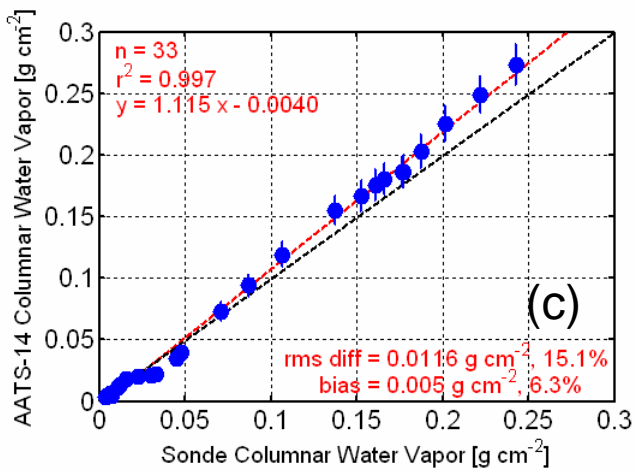
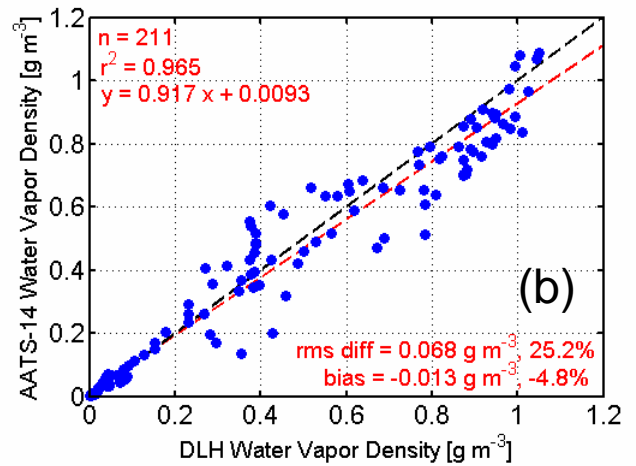
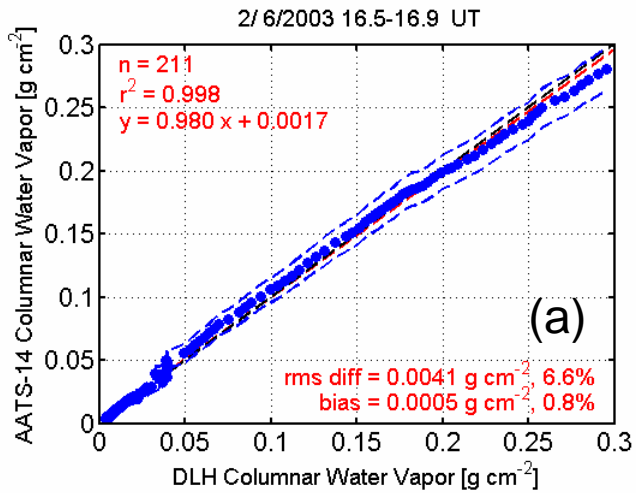


**Fig. 4.** For the 6 February 2003 DC-8 descent into Edwards AFB, scatterplots of AATS-14 versus DLH (a) CWV and (b) water vapor density, and AATS-14 versus Edwards AFB 15 UT radiosonde (c) CWV and (d) water vapor density. Black dashed lines represent one-to-one correspondence, and red dashed lines are the regression fits.

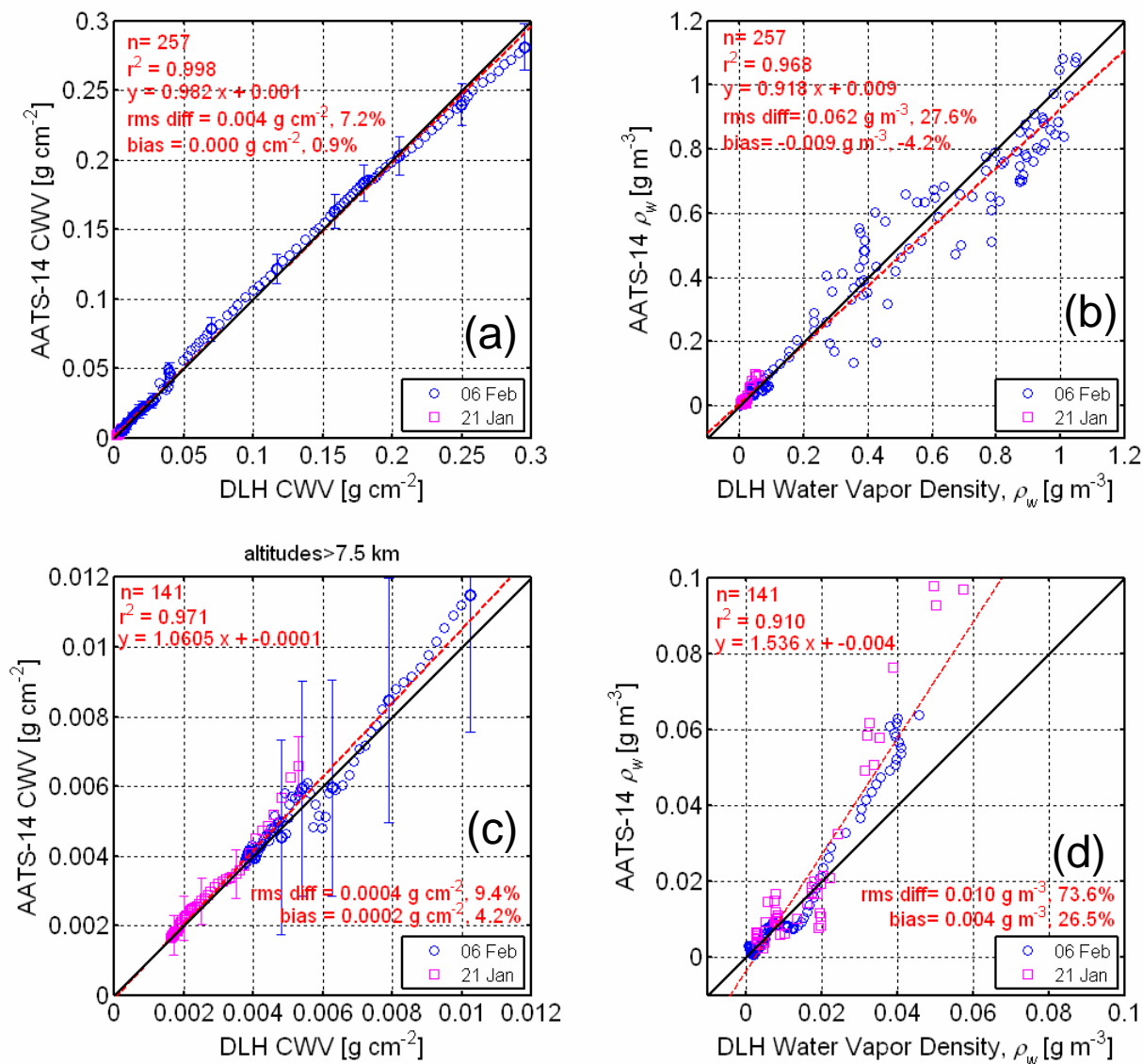


**Fig. 5.** Composite results for the 21 January 2003 ascent and the 6 February 2003 DC-8 descent: scatterplots of AATS-14 versus DLH (a) CWV and (b) water vapor density; scatterplots of AATS-14 versus DLH (c) CWV and (d) water vapor density for altitudes >7.5 km only.